Supporting Information

NIR-emitting and Photo-thermal Active Nanogold as Mitochondria-Specific Probes

Sabyasachi Chakrabortty,[a,b] *Miguel Sison,*[c] *Yuzhou Wu,*[a,b] *Anita Ladenburger,*[d] *Goutam Pramanik,*[a] *Johannes Biskupek,*[d] *Jerome Extermann,*[c] *Ute Kaiser,*[d] *Theo Lasser* [c] *and Tanja Weil* [a,b,*]

[a]Department of Organic Chemistry III, Ulm University, Albert-Einstein-Allee 11, D-89081, Ulm, Germany.

[b]Max-Planck-Institute for Polymer Research, Ackermannweg 10, 55128 Mainz, Germany.

[c]E´cole Polytechnique Fe´de´rale de Lausanne, Laboratoire d'Optique Biome´dicale, CH-1015 Lausanne, Switzerland.

[d]Central Facility of Electron Microscopy, University of Ulm, Albert-Einstein-Allee 11, D-89081 Ulm, Germany.

[e]Hepia, University of Applied Sciences of Western Switzerland (HES-SO), 4 rue de la Prairie, CH-1202 Genève, Switzerland

E-mail: weil@mpip-mainz.mpg.de; tanja.weil@uni-ulm.de

Content:

1. Materials and Instruments

Materials:

Human Serum Albumin >96% (HSA), O-(2-Maleimidoethyl)-O'-methyl-polyethylene glycol 5000 >90% (PEO-5000-MI), N-(2-aminoethyl)maleimide trifluoroacetate salt >95% HPLC, N-hydroxy-succinimide (NHS), Tris(2-carboxy-ethyl)phosphine hydrochloride (TCEP), Urea 98+%, ethylenediaminetetraacetic acid anhydrous (EDTA) >98.5%, (3-Carboxypropyl)triphenylphosphonium bromide (TPP) 98% were all received from Sigma-Aldrich, Hydrogen tetrachloro Aurate (III) trihydrate, ACS, 99.99% was obtained from Alfa Aesar. Sodium borohydride 98% was bought from Acros Organics. Na_2HPO_4, NaH_2PO_4, NaCl and $NaHCO_3$ ACS reagent grade were obtained from Goodrich Chemical Enterprise. cHSA and cHSA-PEO have been synthesized following the procedure reported previously by our group.[1] All chemicals were used as received without further purification. Bio-Rad Bio-Gel P30 was used for desalting column, vivaspin ultrafiltration tubes were purchased from GE healthcare. Ultra-pure Milli-Q water was used for all experiments involving water.

Instruments:

Emission and absorption were recorded using TECAN infinite M1000 microplate reader. Fluorescence quantum yields were measured in Greiner Germany 1534 well μclear transperent microplate. ÄKTA Explore FPLC and SuperoseTM 6 10/30 gel filtration column was used for cHSA-PEO hybrid purification. Precast NuPAGE TA 3%-8% Gel was purchased from Invitrogen and gel electrophoresis was performed in Invitrogen NovekTM Mini-Cell. Zeta-potential and DLS measurements were performed using a Malvern Zetasizer ZEN3600 (Malvern Ltd, Malvern, UK) at 20°C.

TEM:

A JEOL 1400 Transmissions electron microscope was used to obtain bright field TEM images of the larger Au NPs. The aberration-corrected HRTEM imaging was carried out using an image side Cs-corrected FEI Titan 80–300 transmission electron microscope operated at 80 kV acceleration voltage. Images were recorded on a slow-scan CCD-camera type Gatan Ultrascsan XP1000 (FEI Titan). All experiments were carried out at room temperature. STEM was carried out using a FEI 80-300 Titan transmission electron microscope operated at 80kV and equipped with a Fischione high angle annular dark field detector (HAADF) with variable camera length for tunable contrast.

OCM:

Photo thermal imaging of the gold nanoparticles was done using the photo thermal optical lock-in optical coherence microscope (pole-OCM) developed by Pache et al[2]. We use a laser at 532nm

(close to the plasmonic resonance of gold) to illuminate and heat up the nanoparticles. The gold nanoparticles inside the cells then serve as localized heating zones which changes the refractive index of its surrounding. By modulating the heating laser at a fixed frequency we can exploit the lock-in effect and selectively image the regions within the cells that respond to the heating. Furthermore, by adding a fluorescence imaging modality to the poli-OCM we are able to transition between poli-OCM and fluorescence confocal imaging within the same instrument instantly. This modality allows us to compare fluorescence and photothermal imaging.

Fluorescence confocal imaging was done at a single axial position which means only two dimensional fluorescence data is available. Using the Mitotracker DeepRed dye, the fluorescence images show, in two dimensions, where the mitochondria are located within the cell. Meanwhile, photothermal imaging with the poli-OCM provides full three-dimensional images and to compare the information from the two different techniques we take the maximum intensity projection of the full three-dimensional tomogram along the axial direction.

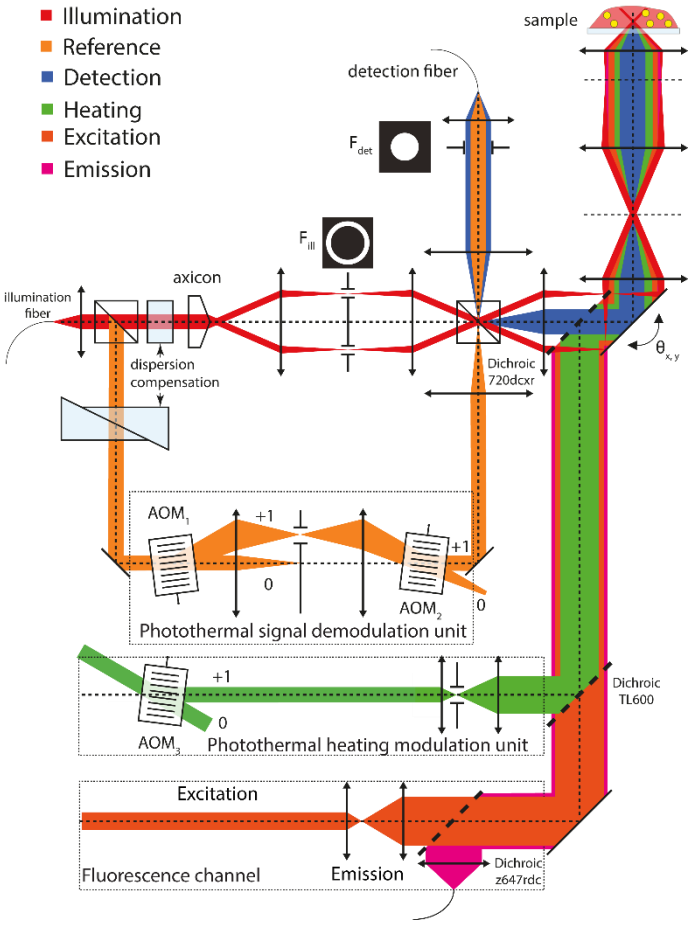

Scheme S1. poli-OCM setup with fluorescence channel for co-localization of photo-thermal and fluorescence imaging.

2. **Synthesis and characterization of albumin derived polypeptide**

Synthesis of dcHSA-PEO-TAT (5):

dcHSA-PEO (**4**) (2 mg) was dissolved in PBS buffer (1 mL, pH 7.4) before addition of MI-NHS (3 mg, MW-308.29) into it. Then, this mixture was stirred at room temperature for about 4 h. Finally, it was ultra-centrifuged and concentrated to 200 µL. Subsequently, a solution of TAT (3 mg) in PBS buffer (2 mL, pH 7.4) was added to this NHS activated **4**, and reacted overnight. The final solution yielded **5** and washed several times in water to get rid of unreacted TAT peptide and kept at 4 °C.

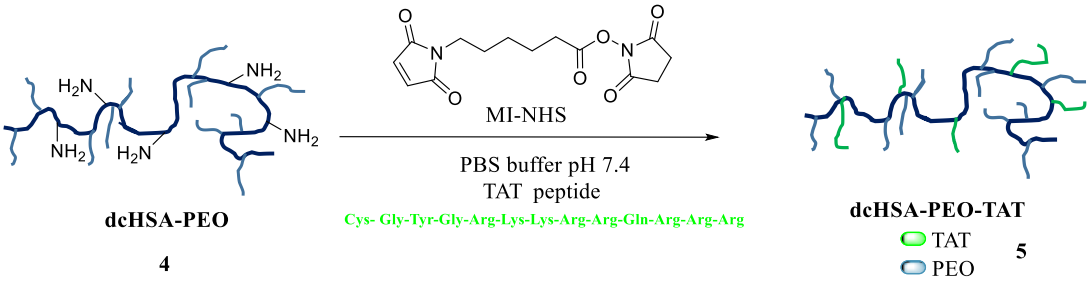

Scheme S2. Synthetic scheme for **5**.

Synthesis of dcHSA-PEO-TAT-TPP (6):

This reaction was proceeded through EDC coupling pathway. First, TPP (8 mg), NHS (3 mg) and EDC.HCl (4 mg) was dissolved and degassed in 0.5 mL of DMF solution. This mixture was stirred overnight at room temperature under argon atmosphere. The next day, dcHSA-PEO-TAT (**5**) (2 mg) dissolved in 2 mL Milli-Q water was added and again reacted overnight at room temperature. Finally, the product was washed through vivaspin 20 (MWCO 30K) ultracentrifuge tube to separate unreacted reactants. Finally, it was kept at 4 °C for future use.

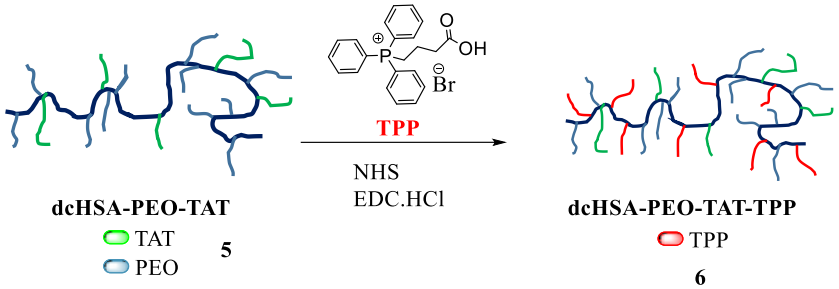

Scheme S3. Synthetic scheme for **6**.

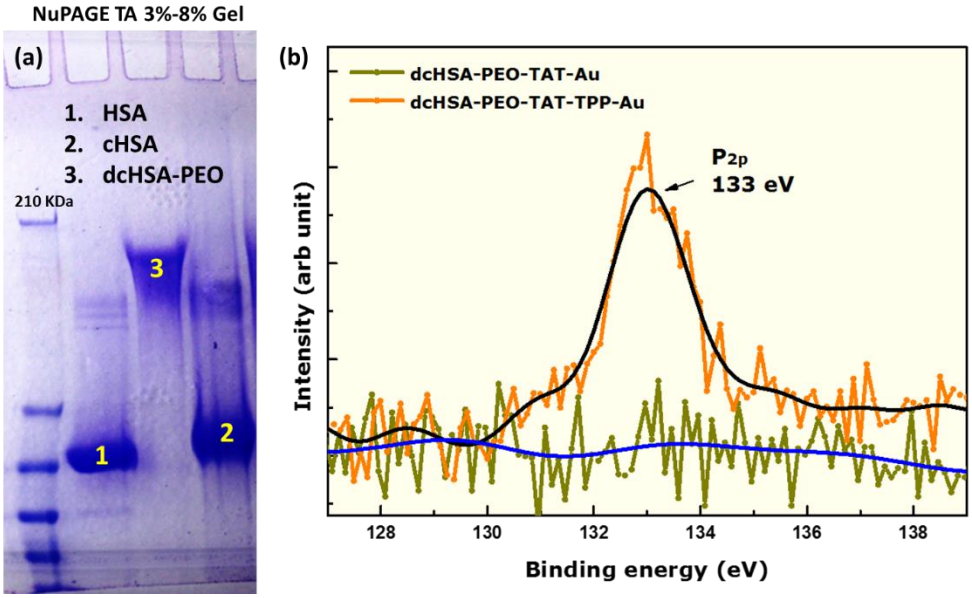

Figure S1. (a) SDS-PAGE analysis of HSA, cHSA, dcHSA-PEO hybrid. From this gel image, progressive increase in molecular weight clearly proves successful conjugation at each step. (b) High resolution XPS spectrum of P_{2p}, the fitted peak positions (black solid line) of dcHSA-PEO-TAT-TPP-Au construct where the presence of phosphorus signal was clearly evident. On the other hand, hybrid with missing TPP (dcHSA-PEO-TAT-Au) unit showed no phosphorous signal.

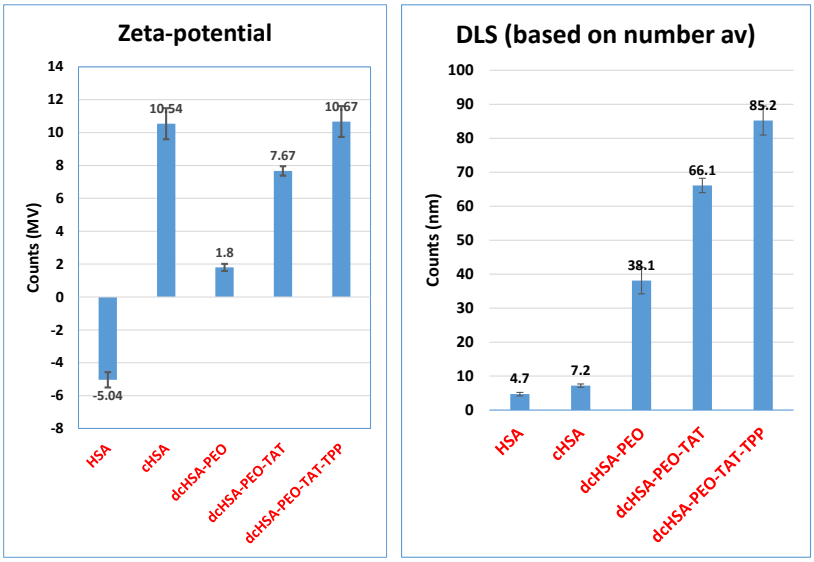

Figure S2. Zeta-potential and dynamic light scattering values of HSA, cHSA, dcHSA-PEO, dcHSA-PEO-TAT and dcHSA-PEO-TAT-TPP conjugates. Increase in zeta-potential as well as relative size prove the efficiency of each reaction step where different functional moieties are attached.

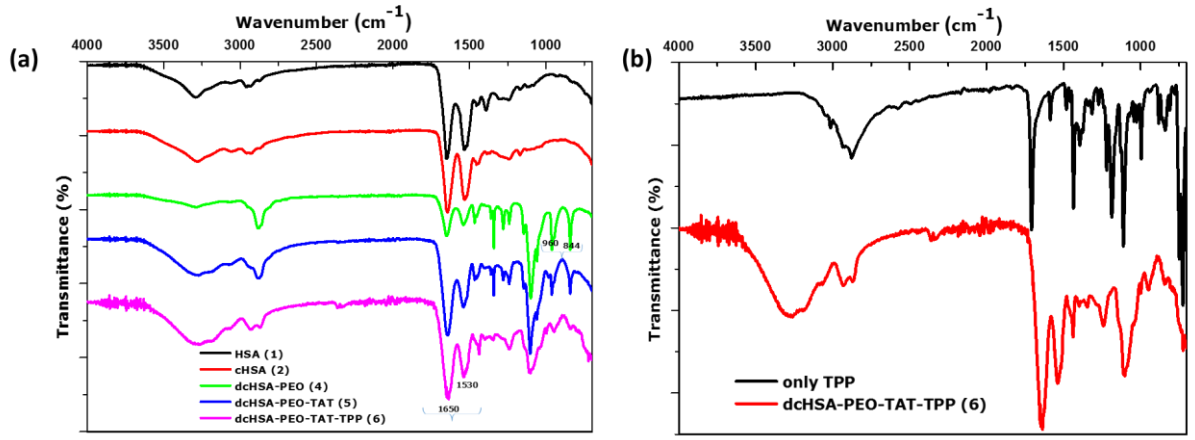

Figure S3. IR spectra of synthesized different protein conjugates. The presence of IR bands for each structure at 1650 cm^{-1} and 1530 cm^{-1} are corresponding to amide I and amide II bands in protein structures respectively. This shows highly stable nature of the polypetide backbone while treated with several reaction conditions. In addition, the bands at 960 cm^{-1} and 844 cm^{-1} in **4** are the characteristics of primary amine. Slow, disappearance of these bands in **5** and **6** are the indication of attachment of TAT and TPP on the polypetide structure as we used primary amine centers to react for attachment of TAT and TPP.

Synthesis of dcHSA-PEO-TPP:

This reaction was proceeded through EDC coupling pathway. First, TPP (8 mg), NHS (3 mg) and EDC.HCl (4 mg) was dissolved and degassed in 0.5 mL of DMF solution. This mixture was stirred overnight at room temperature under argon atmosphere. Next day, dcHSA-PEO (**4**) (2 mg) dissolved in 2 mL Milli-Q water was added and again reacted at room temperature for overnight. Finally, the product was washed through vivaspin 20 (MWCO 30K) ultracentrifuge tube to separate unreacted reactants. Finally, it was kept at 4 °C for future use.

Synthesis of dHSA-PEO-TAT-TPP:

This reaction was proceeded exactly the same way as **6**, expect the cationization step of the HSA protein was not performed initially.

3. **Synthesis of ultra-small Au NPs**

Protein templated:

Synthesis of monodispersed ultra-small Au NPs proceeded based on a previously reported procedure with slight modifications.[3] In a typical experiment, freshly prepared aqueous $HAuCl_4$ solution (2 µL, 10 mM) was added to dcHSA-PEO-TAT-TPP solution (20 µL, 7 mg/mL) in a 1.5 mL Eppendorf tube. This mixture was then shaken vigorously at 37 °C for about 5 min. Finally, NaOH solution (1 µL, 1 M) was introduced and the reaction was allowed to proceed under vigorous shaking

at 37 °C for 24 h. As synthesized, Au NPs were washed through ultracentrifuge to remove excess base, and kept under 4 °C for future use. These particles were characterized through TEM.

To synthesize small Au NPs with various other protein backbone functionalization, such as, dcHSA-PEO-TPP (no TAT), dHSA-PEO-TAT-TPP (not cationic HSA) and dcHSA-PEO-TAT (no TPP) were followed the similar pathways as described above; where the same concentration of these proteins was used as template.

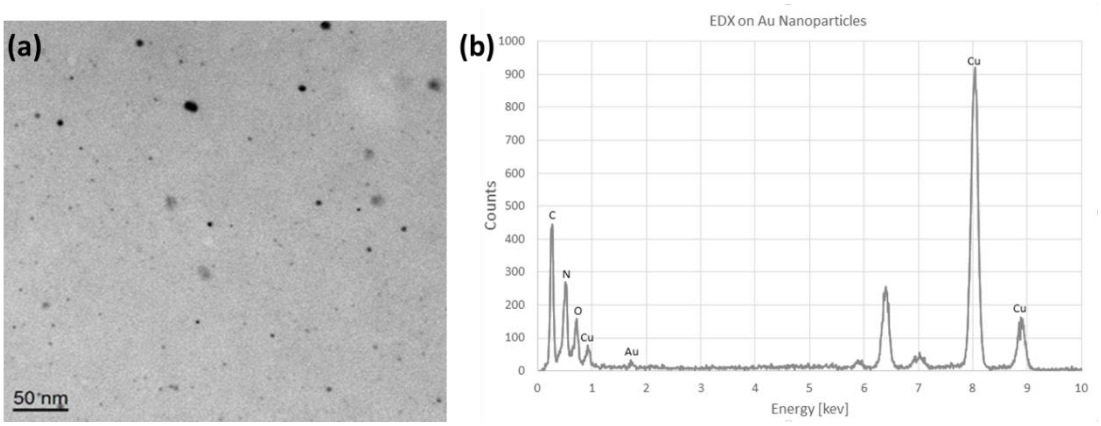

Figure S4. (a) Representative TEM image of a large field view of small Au NPs present in the solution, where the size of the particles is 2.0 ± 0.5 nm. The occasional existence of lager particles is believed to be the aggregation of tiny Au NPs, as otherwise we observed the presence of well-dispersed, highly stable, small Au NPs. (b) EDX spectra taken from the TEM grid, clearly confirms the presence of Au and N in the sample.

NaBH4 reduction method:

Typically, $HAuCl_4.3H_2O$ (10 µL, 50.8 mM) solution and required volume of **6** conjugates was added together and the solution was diluted to 250 µL Milli-Q water and then the mixture was stirred at room temperature for 1h. Then freshly prepared $NaBH_4$ solution in chilled deionized water was added dropwise to the solution mixture and it was stirred overnight. Always excess of NaBH4 was used to ensure that all the Au (III) reduced to Au (0). As synthesized, Au NPs were washed through ultracentrifuge to remove excess NaBH4, and kept under 4 °C for future use.

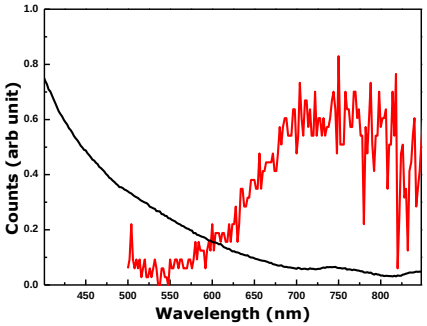

Figure S5. Representative absorption and emission spectra of prepared small Au NPs by $NaBH_4$ reduction method. Poor quantum yield corresponds to weak fluorescent signal present in emission spectra.

4. **Stability test under various physiological condition and cytotoxicity test**:

Since, we use these NPs for intracellular studies, it is very important to study their stability under cellular environment. We have tried to observe in particular, their fluorescent behavior after 24 h incubation with various physiological conditions. Since, there were no observable features present in absorption spectra, we purposefully excluded those spectra while comparing. In all cases, they showed excellent stability and no aggregation was observed while comparing their emission spectra. Furthermore, we have tested their toxicity effect with HeLa cells and it was found that in our imaging conditions most of the cells were viable for both small and large Au NPs.

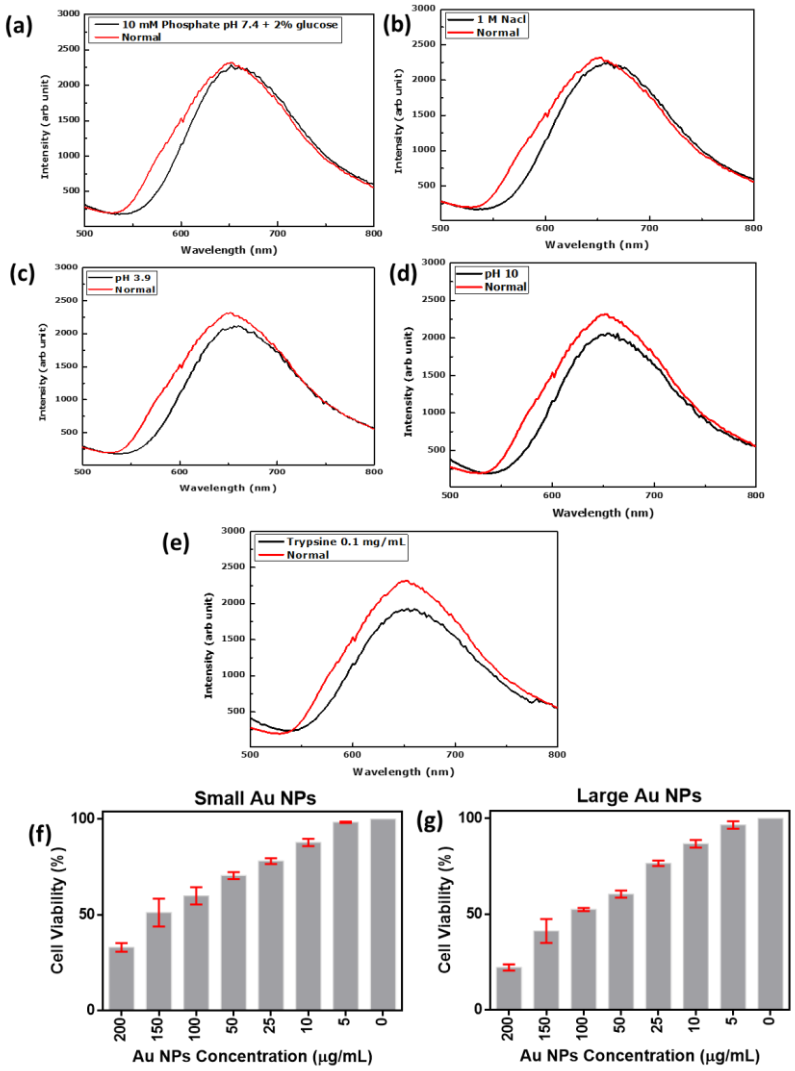

Figure S6. Stability test of Au NPs coated with dcHSA-PEO-TAT-TPP in different solutions (30% v/v). (a) 10mM Phosphate buffer pH 7.4 +2% glucose solution, (b) 1M NaCl, (c) pH 3.9, (d) pH 10 and (e) Trypsine. All solutions were excited at 365 nm. Even after 24 h of incubation, the emission intensity of these Au NPs remain almost unchanged in all the situation and also no precipitation of Au NPs was observed. This indicates the remarkably high colloidal stability of these hybrids. (e-f) Cell viability test showing more than 90% viable Hela cells incubated with either small or large of

mitochondria targeting AuNPs in our imaging conditions (both the cases we used ~ 5 µg/mL Au NPs solution).

5. **Control experiments for synergistic effect**:

To ascertain the synergistic effect of cationic-HSA and attachment of TAT peptide on efficient cellular uptake process, confocal studies with dcHSA-PEO-TPP (i.e., no TAT attachment) (Figure S7) and dHSA-PEO-TAT-TPP (i.e., without the use of cationicHSA) (Figure S8) were performed. Each case we have prepared small, NIR emitting Au NPs, where they showed emission max ~690 nm. Each sample is incubated with HeLa cells for 18 h before imaging.

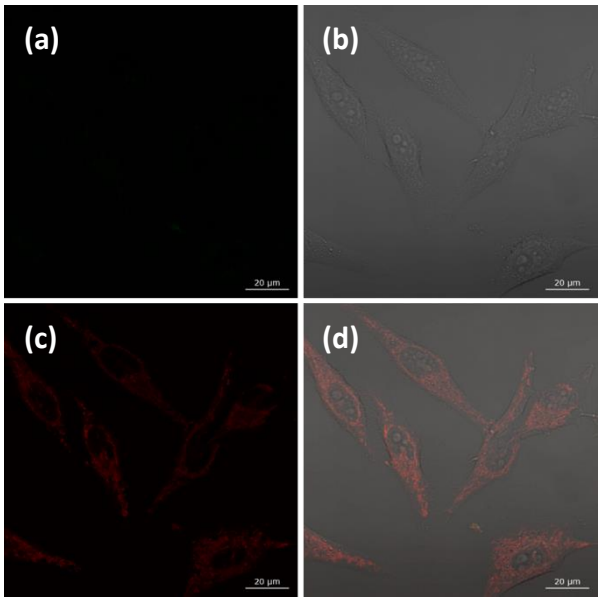

Figure S7. Confocal microscopy image of HeLa cells incubated with dcHSA-PEO-TPP-Au NPs. (a) Represents data acquired by the Au NPs channel. (b) DIC image (c) Red spots represent, data acquired by the MitoTrackerR Red CM-H2XRos (Invitrogen) channel. (d) Overlay. Image scanned using simultaneous scanning. No observable spots presents for (a), indicating no uptake of the hybrids.

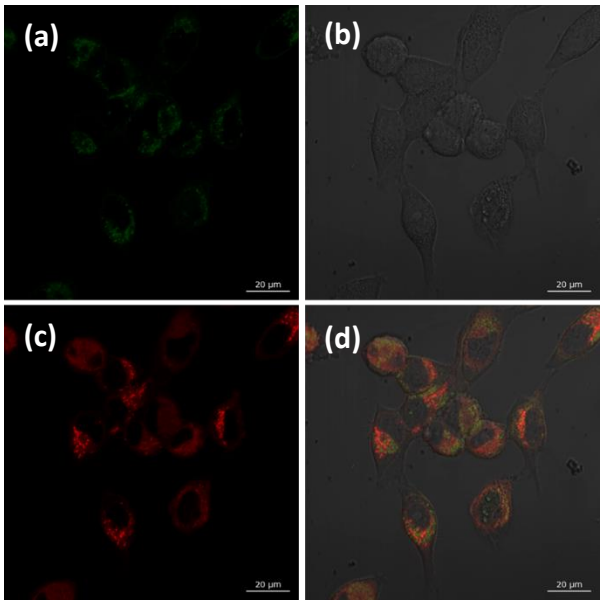

Figure S8. Confocal microscopy image of Hela cells incubated with dHSA-PEO-TAT-TPP-Au NPs. (a) Little green spots represent, data acquired by the Au NPs channel. (b) DIC image (c) Red spots represent, data acquired by the MitoTrackerR Red CM-H2XRos (Invitrogen) channel. (d) Overlay. Image scanned using simultaneous scanning. Although, little presence of green dots indicate poor uptake, the overlay image show almost no overlap with mito-tracker.

From the observation of these two images taken together, it is very clear that both the presence of cationic polypeptide (cHSA) and TAT peptide are of absolute necessity for efficient intracellular uptake.

6. **Control experiment for better endosomal release**:

With the help of TAT peptide, better endosomal release was observed. When larger Au NPs are passivated by peptide dcHSA, without TAT attachment, most of the Au NPs stayed in endosomal region. This was characterized by TEM.

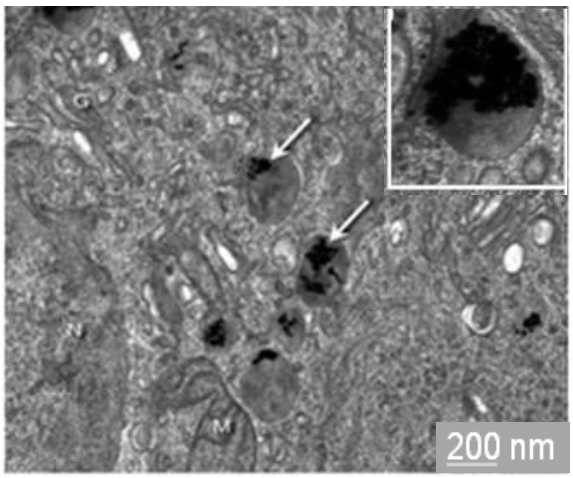

Figure S9. TEM image of thin section of Hela cells, incubated with dcHSA coated Au NPs for 24h and the Au NPs are usually found mostly in endosomes.

7. **Confocal study with dcHSA-PEO-TAT-Au**:

We investigated the effectiveness of TAT peptide towards mitochondria co-localization. We have synthesized small fluorescent Au NPs with dcHSA-PEO-TAT as polypeptide coating. Although, TAT peptide known for mitochondria targeting capabilities,[4] we observed nearly no overlap occurred with TAT only targeting group. Thus, it can unambiguously be concluded that the presence of lipophilic cation, TPP enhances mitochondria targeting capabilities by a great extent.

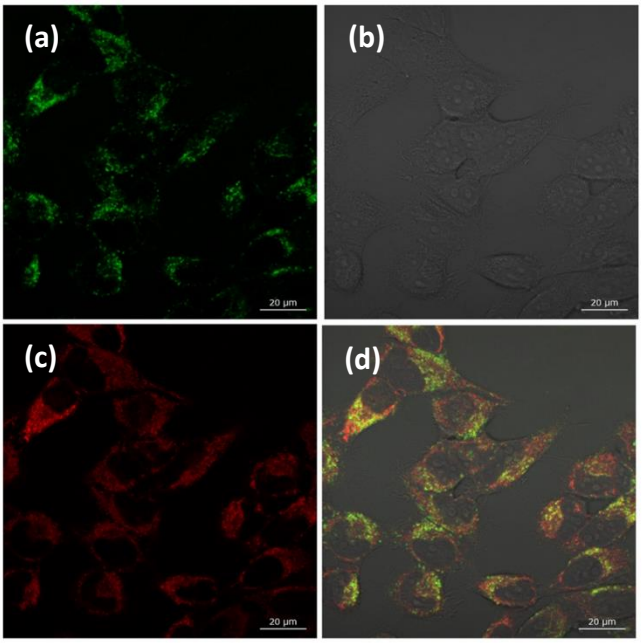

Figure S10. Confocal microscopy image of Hela cells incubated with dcHSA-PEO-TAT-Au NPs. (a) Green spots represent, data acquired by the Au NPs channel. (b) DIC image (c) Red spots represent, data acquired by the MitoTrackerR Red CM-H2XRos (Invitrogen) channel. (d) Overlay. Image scanned using simultaneous scanning. Although, several green dots indicate better uptake, the overlay image show almost no overlap with mito-tracker.

8. **Synthesis, characterization and poli-OCM study of non-fluorescent, larger Au NPs**:

Relatively large Au NPs are synthesized for their use in OCM analysis. Briefly, aqueous $HAuCl_4$ solution (60 µL, 10 mM) and polypeptide polymer dcHSA-PEO-TAT-TPP (50 µL, 7 mg/mL) was added together and the solution was diluted to 250 µL with Milli-Q water. Next, freshly prepared $NaBH_4$ solution (6 µL, 3 mg/mL) in chilled Milli-Q water was added rapidly to the solution mixture. Then the reaction mixture was stirred for 30 min before washing. Finally, Au NPs was characterized by UV-Vis and TEM.

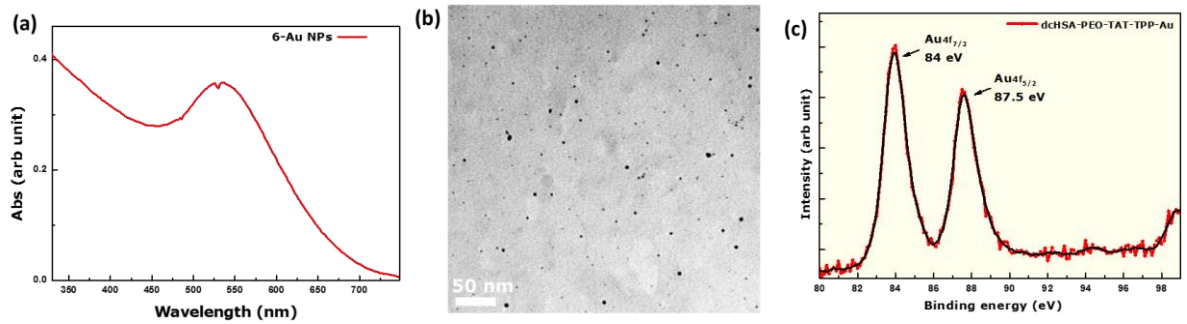

Figure S11. (a) Absorption spectra of the Au NPs prepared by $NaBH_4$ reduction. A clear hump indicates these nanoparticles are not ultra-small. (b) Representative TEM image of these Au NPs, showing nice colloidal stability and they are in the size range of 4 ± 1.3 nm. (c) High-resolution XPS spectrum showed clear Au4f7/2 and Au4f5/2 signals, proving the existence of Au in the sample.

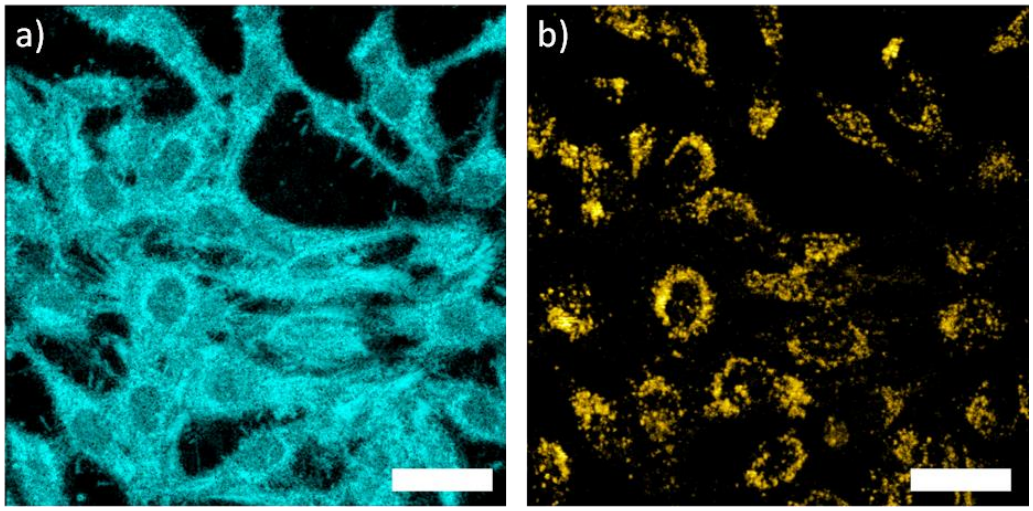

Figure S12. Axial projection from 3D (a) df-OCM and (b) poli-OCM images where 50 µL of dcHSA-PEO-TAT-TPP coated Au NPs were used. The poli-OCM image in (b) clearly demonstrate the specific contrast of poli-OCM imaging with AuNPs. Scale bar 30µm.

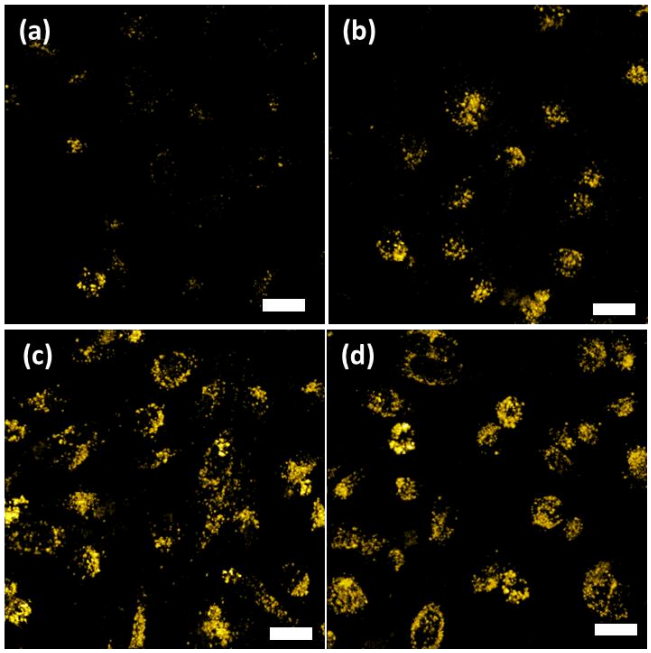

Figure S13. Axial projection (a-e) poli-OCM images, with 2, 5, 10 and 25 µL of dcHSA-PEO-TAT-TPP coated Au NPs. A clear indication of increased signals is evident. Scale bar 20µm.

Poli-OCM experiment conditions:

Hela cell were incubated over a 12hr period with varying concentrations of AuNPs mixed within the culture media. Imaging was performed using the dual modality of the poli-OCM which allowed us to image the complete 3D cell morphology in the dark-field OCM mode (figure S12(a)) whereas the poli-OCM mode specifically imaged the AuNPs inside (figure S12(b)). We were able to image living cells with the aid of a custom built microincubator with temperature controlled at 37°C and pumped with humidified premixed air (5% CO_2). The poli-OCM utilizes a femtosecond laser with a central wavelength at 800nm and bandwidth of 130nm as its probe beam and a photothermal heating beam at 532nm; for imaging these lasers had a power of 6.5mW and 3mW respectively.

The deduced photothermal scattering signal can be written as[5]

$$S \approx \frac{1}{\pi\omega_0 C_P \lambda^2 \Omega} n \frac{\partial n}{\partial T} \frac{\sigma_{abs}}{A} P_{heat} P_{probe} \Delta t,$$

…….. Equation S1

where Δt is the detector integration time, ω_0, λ, and P_{probe} are the radius, wavelength, and power of the probe beam respectively, Cp is the heat capacity per unit volume of the medium with n as its refractive index changing with temperature following $\partial n/\partial T$. The heating beam modulation frequency is given by Ω with a power given by P_{heat}. The last factor gives the ratio between the absorption cross section, σ_{abs}, of the Au NPs and the diffraction limited spot area, A, of the photothermal heating beam. Following this equation, optimizing the scattering signal in photothermal microscopy benefits greatly from increasing the absorption cross section of the AuNPs.

References:

1. Y. Wu, G. Pramanik, K. Eisele and T. Weil, *Biomacromolecules*, 2012, **13**, 1890–1898.

2. C. Pache, N. L. Bocchio, A. Bouwens, M. Villiger, C. Berclaz, J. Goulley, M. I. Gibson, C. Santschi and T. Lasser, *Opt. Express* 2012, **20**, 21385.

3. J. Xie, Y. Zheng and J. Y. Ying, *J. Am. Chem. Soc.*, 2009, **131**, 888–889.

4. V. D. Gaizo and R. M. Payne, *Mol. Ther.*, 2003, **7**, 720–730.

5. A. Gaiduk, P. V. Ruijgrok, M. Yorulmaza and M. Orrit, *Chem. Sci.*, 2010, **1**, 343-350.